

Timing the starburst-AGN connection

Vivienne Wild^{1*}, Timothy Heckman², Stéphane Charlot¹

¹ *Institut d'Astrophysique de Paris, CNRS, Université Pierre & Marie Curie, UMR 7095, 98bis bd Arago, 75014 Paris, France*

² *Department of Physics and Astronomy, Johns Hopkins University, Baltimore, MD 21218, USA*

28 October 2021

ABSTRACT

The mass of super massive black holes at the center of galaxies is tightly correlated with the mass of the galaxy bulges which host them. This observed correlation implies a mechanism of joint growth, but the precise physical processes responsible are a matter of some debate. Here we report on the growth of black holes in 400 local galactic bulges which have experienced a strong burst of star formation in the past 600 Myr. The black holes in our sample have typical masses of $10^{6.5} - 10^{7.5} M_{\odot}$ and the active nuclei have bolometric luminosities of order $10^{42} - 10^{44}$ erg/s. We combine stellar continuum indices with $H\alpha$ luminosities to measure a decay timescale of ~ 300 Myr for the decline in star formation after a starburst. During the first 600 Myr after a starburst, the black holes in our sample increase their mass by on-average 5% and the total mass of stars formed is about 10^3 times the total mass accreted onto the black hole. This ratio is similar to the ratio of stellar to black hole mass observed in present-day bulges. We find that the average rate of accretion of matter onto the black hole rises steeply roughly 250 Myr after the onset of the starburst. We show that our results are consistent with a simple model in which 0.5% of the mass lost by intermediate mass stars in the bulge is accreted by the black hole, but with a suppression in the efficiency of black hole growth at early times plausibly caused by supernova feedback, which is stronger at earlier times. We suggest this picture may be more generally applicable to black hole growth, and could help explain the strong correlation between bulge and black hole mass.

Key words: galaxies: starburst, active, bulges

1 INTRODUCTION

The existence of a strong correlation between the masses of supermassive black holes and the galactic bulges where they reside is strongly suggestive of a mechanism of joint growth (Gebhardt et al. 2000; Ferrarese & Merritt 2000; Tremaine et al. 2002). However, the physical mechanism(s) responsible for this observed relation remain unclear (Ferrarese & Ford 2005; Cattaneo et al. 2009). The very different physical scales involved in building bulges through star formation and feeding a central black hole pose a great challenge for the possible mechanisms of causal connection. Several theoretical models successfully reproduce the observed relation, (e.g. Silk & Rees 1998; Haehnelt et al. 1998; Hopkins et al. 2006; Ciotti & Ostriker 2007; Khalatyan et al. 2008), most invoking some form of “feedback” by which the energy radiated during the phase of rapid accretion onto the black hole prevents further accretion and shuts down star formation. However, observationally there is little evidence for effective direct “mechanical” feedback caused exclusively by energy released during accretion onto the black hole.

Clues to the nature of the relationship between the growth of

bulges and black holes have been provided over the last decade through the significant observational progress that has been made in understanding the demographics of the AGN population and its relationship to the properties of the host galaxies. In the local Universe, the Sloan Digital Sky Survey (SDSS) spectroscopic survey (York et al. 2000; Strauss et al. 2002; Abazajian et al. 2009) has provided the statistics necessary to calculate volume averaged quantities and to reveal which populations of AGN and galaxies are the sites of the majority of present day black hole growth. Kauffmann et al. (2003) showed that significant growth of black holes is presently happening in galaxies with the masses and structural properties of early-type galaxies, but with significant amounts of recent or on-going star-formation. Heckman et al. (2004) then found that the majority of low-redshift black hole growth occurs in high growth rate phases (L/L_{Edd} greater than a few percent) which must be of short duration relative to the Hubble time. This is consistent with the fact that integrating the luminous output of quasars (high L/L_{Edd} accretors) over all cosmic times gives a black hole mass density similar to that observed in the local Universe (Yu & Tremaine 2002). Comparing the integrated ongoing starformation to the integrated ongoing black hole accretion, Heckman et al. (2004) found a value close to that expected from the $M_{\text{BH}} - M_{\text{bulge}}$ relation, implying that bulge formation and BH

* wild@iap.fr

growth are still tightly coupled even today. However, rapid growth of the population of bulges and their black holes is occurring today only in systems of relatively low-mass (so-called cosmic downsizing).

One long-standing idea linking the evolution of bulges and black holes is that there is a strong evolutionary connection between intense central bursts of star formation and the growth of black holes. In Wild et al. (2007) we found that in fact the majority of the most rapidly growing black holes at the present day exist in star-forming galaxies with bulges, but with relatively ordinary recent star formation histories and no indication of a recent strong burst of star formation. However, we also found that galaxies which are undergoing or have recently undergone the strongest bursts of star formation in the sample showed an increased probability of hosting a rapidly growing black hole. This link between strong starburst and black hole growth may have been more important at higher redshifts where gas was more abundant (potentially leading to larger and more frequent bursts of star formation), and where the majority of the black hole mass in the universe was accreted.

Progress on understanding the link between star formation and black hole growth has also been provided by detailed observations of very nearby AGN which can probe spatial scales of 10s to 100s of parsecs (an order of magnitude smaller than the typical scale probed by the 3" SDSS fibre aperture). Evidence for young nuclear stellar populations is found in around half of local AGN studied (see Davies et al. 2007, for a recent summary of the literature). In the future such an approach may be extended to provide a systematic investigation covering several orders of magnitude in bolometric luminosity and black hole mass, and including starbursts with no current black hole growth. Of direct importance to this paper is the discovery of a possible delay between the peak of the starburst and AGN activity for a handful of nearby AGN (Tadhunter et al. 1996; Emonts et al. 2006; Goto 2006; Davies et al. 2007). Such a delay may also be related to the very low accretion rate observed in the Galactic center (Baganoff et al. 2003), despite the presence of considerable wind material from young OB stars (Paumard et al. 2006). Schawinski et al. (2007) used the Lick indices and photometry of a morphologically selected sample of elliptical galaxies to reveal that those with emission lines dominated by star formation typically have more recent star formation than those with emission lines dominated by AGN. They interpreted this as a delay between starformation and AGN activity. However, they neglect the fact that more recent star formation will hide increasingly powerful AGN, which will significantly affect their result.

In this paper we bridge the gap between the gross trends of stellar populations with AGN properties uncovered by SDSS, and detailed studies of the recent star formation in the nuclei of local AGN. We use the SDSS to select the galaxies with bulges which have recently undergone the strongest bursts of starformation in the local Universe. Our sample is complete for ages up to 600 Myr after the onset of the starburst, considerably longer than the typical timescale for black hole accretion events. From this sample, we construct a time-averaged view of black hole accretion subsequent to a star formation episode.

In Section 2 we present the sample and the method used to measure the age of the starburst from the stellar continuum. In Section 3 we derive black hole accretion rates and instantaneous star formation rates from the emission line fluxes, and quantify the completeness of our samples. The results are presented in Section 4 and discussed in Section 5. Throughout the paper, we calculate luminosities using $\Omega_M = 0.3$, $\Omega_\Lambda = 0.7$ and $H_0 = 70\text{km/s/Mpc}$.

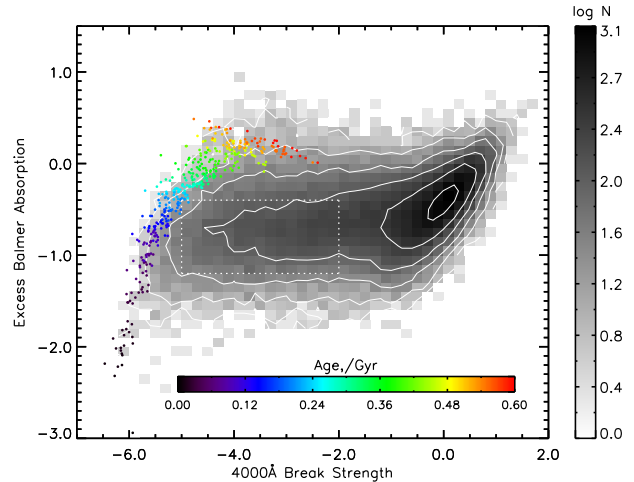


Figure 1. The distribution of 4000Å break strength and Balmer absorption line strength for 70,000 bulge-galaxies (grayscale, in logarithmic number). The spectral indices are generated using a Principal Component Analysis of a model spectral library as described in Wild et al. (2007). The star formation histories of galaxies that lie in different regions of the diagram are described in Section 2. The starburst sample is overplotted as coloured dots, where colour indicates the age of the starburst. The dotted box indicates the region from which the starforming comparison sample is drawn.

For the reader who is less interested in the technical aspects of this work we recommend reading the introductions to Sections 2 and 3 (i.e. skipping the subsections), before moving onto the results and conclusions.

2 A LOCAL STARBURST SAMPLE

AGN (the observational manifestation of growing black holes) are found in galaxies with bulges, from early type spirals through to massive ellipticals (Ho et al. 1997; Dunlop et al. 2003; Kauffmann et al. 2003; but see Filippenko & Ho 2003 for an exception). Therefore we select as our starting point a base sample of $\sim 70,000$ galaxies from the Sloan Digital Sky Survey (SDSS) data release 7 (Abazajian et al. 2009), selected to have high stellar surface mass densities characteristic of bulges (Kauffmann et al. 2003). We restrict the sample to galaxies with redshifts $0.01 < z < 0.07$. At these redshifts the 3 arcsec aperture of the SDSS optical fibres samples the inner $\lesssim 2\text{kpc}$ radius of the galaxies, so that light from the stars in the bulge dominates the spectrum (Gadotti 2009). Broad-line (i.e. Type 1 or unobscured) AGN are not included in our sample, as light from the central nucleus would contaminate our study of the stellar population in the host galaxy. Full details of the sample selection criteria are given in the following subsection, in the remainder of this section we introduce the concept of our methodology.

In the integrated spectrum of a galaxy the different signatures of stars of different ages can be used to obtain information about a galaxy’s recent star formation history. In Fig. 1 we begin by inspecting the distribution of two common stellar continuum indices for the 70,000 bulge-galaxies, the 4000Å break strength and the excess Balmer absorption line strength (Wild et al. 2007). The majority of bulge-galaxies show no evidence of recent or current star formation, they form the “red-sequence” which lies on the right, with strong 4000Å break strength indicating that the galaxies contain

predominantly old stars. There is a significant minority of bulge-galaxies that are forming stars, these have younger mean stellar ages and therefore weaker 4000Å break strengths and form the “blue-sequence”. A small number of bulge-galaxies are undergoing a “starburst” i.e. there has been a sharp increase in the galaxy’s star formation rate over a timescale that is short ($\sim 10^8$ years) in comparison to the age of the galaxy. They differ from blue-sequence galaxies only in the strength and/or short timescales of the star formation episode. These galaxies are identified by their unusually weak Balmer absorption lines, strong UV-blue continua, and weak 4000Å breaks i.e. spectra dominated by light from O/B stars. These objects lie in the lower left of Fig. 1. As the starburst ages, the Balmer absorption lines increase in strength as the galaxy passes into the post-starburst phase (Dressler & Gunn 1983; Couch & Sharples 1987), i.e. A/F star light dominates the integrated galaxy spectrum. These objects lie in the upper left of the figure. The shape of the left hand side of the distribution in Fig. 1 therefore describes the evolutionary track of a starburst galaxy, with time since the starburst increasing from bottom to top, and burst strength increasing from right to left (Couch & Sharples 1987; Kauffmann et al. 2003; Wild et al. 2007). Thus the evolution of the strongest starbursts that occur in bulges in the local Universe defines the outer lefthand edge of the distribution.

The unique advantage of our sample for timing the starburst-AGN connection is that the time since the onset of the starburst can be measured accurately using population synthesis models. For ordinary blue-sequence galaxies, the time since a recent, smaller change in star formation rate is essentially unconstrained using integrated spectra alone, making a similar measurement of the relative timing of star formation and black hole growth impossible with the data in hand.

To sample the properties of AGN in different evolutionary stages of the starburst, we select a constant number of the strongest starburst galaxies per unit age. We cannot use our indices to measure the age of starbursts to arbitrarily old ages, firstly because the light from weaker starbursts fades rapidly until they become indistinguishable from ordinary starforming galaxies, and secondly because even the stronger starburst galaxies suffer from a “burst age-mass degeneracy” at late times. We therefore trade maximum burst age against sample statistics in order to select a complete sample of 400 bulge-galaxies which have undergone a starburst in the last 0.6 Gyr. The starburst sample is shown as coloured dots in Fig. 1.

In the following subsections we give further details of the sample selection and the calculation of the age of the starburst.

2.1 Details of the sample selection

Our bulge-galaxy sample contains galaxies with stellar surface mass density $\mu^* = 0.5M^*/\pi \times r^2 > 3 \times 10^8 M_\odot/\text{kpc}^2$, where stellar mass (M^*) is measured from the 5-band SDSS photometry (J. Brinchmann, <http://www.mpa-garching.mpg.de/SDSS>) and radius (r) is calculated from the z -band Petrosian half light radius. Although this selection does not necessarily isolate solely those galaxies with large bulge-to-disk mass ratios, this mass density cut is based on previous results that find that AGN in SDSS are predominantly located in host galaxies with high stellar surface mass density (Kauffmann et al. 2003; Heckman et al. 2004).

We note that our stellar surface mass density cut excludes most, although not all, pseudo-bulges. Recently, Gadotti & Kauffmann (2009) have shown that pseudo-bulges contain 4% of the black hole mass in the local Universe. Empirically, we find that

SDSS galaxies with pseudo-bulges have a slightly lower limit on their stellar surface mass density of $\mu^* > 1 \times 10^8 M_\odot/\text{kpc}^2$ (Gadotti 2009) and therefore we have verified that our conclusions remain unchanged when we use this lower stellar surface mass density limit.

We impose a per-pixel signal-to-noise ratio (SNR) limit on the spectra of 8 in the g -band to ensure accurate measurement of the stellar continuum and emission lines. At these low redshifts and relatively high stellar masses of bulge-galaxies, only 4% of spectra have SNR below this cut and decreasing the limit from 8 to 6 does not alter our conclusions.

We remove galaxies with stellar velocity dispersions < 70 km/s, below which the SDSS spectra have insufficient spectral resolution to measure accurate stellar velocity dispersions and therefore reliable black hole masses. This effectively places a lower limit on black hole mass of $10^{6.3} M_\odot$ (Tremaine et al. 2002), and we emphasise that our results directly pertain only to black holes with masses above this limit. As with any hard cut on sample properties, this cut on stellar velocity dispersion may introduce a small bias into our results: new systems will enter the sample at later times as the black holes grow and cross the sample selection threshold. However, with typical black hole growth factors of 10% (see Section 5) the effect should be small.

Finally, we remove a very small number (five) of candidate “dusty starbursts” which have very large Balmer decrements (> 2.5 times the intrinsic ratio, see below) and are identified as having $H\alpha$ luminosities that are too high for their starburst age. Due to the obscuration of the youngest and hottest stars behind optically thick dust clouds, these dusty but actively star forming galaxies may potentially have continuum spectral indices which place them, incorrectly into the strong-starburst track (Poggianti & Wu 2000, Wild et al. in prep). The inclusion or not of these 5 objects does not alter the conclusions of this paper.

2.2 Measuring starburst age

In order to boost the signal-to-noise ratio of traditional indicators of recent star formation history, in particular the measurement of the Balmer absorption lines, we use indices defined from a Principal Component Analysis (PCA) of the 4000Å break region of the spectra. The full method is described in detail in Wild et al. (2007). To measure the age of the starbursts, we build a model library of 10^7 star formation histories composed of an old bulge population with superposed exponentially decaying starbursts (Bruzual & Charlot 2003, Charlot & Bruzual, in prep). This star formation prescription, in addition to being intuitive for the sample at hand, provides a model library that fully covers the observed distribution of index values and naturally explains the observed shape of the distribution in Fig. 1.

The bulge population is formed from a tophat starburst of 0.5 Gyr width, evolved passively for 13 Gyr. The star formation history of the model bulge population is unimportant, but the age is set to give a precise match to the position of the red-sequence in our stellar continuum indices. The metallicity of all models in the library is fixed to $0.5 Z_\odot$ to agree with the position of the peak of the red-sequence for our galaxy sample. We note that this is slightly lower than generally measured for samples of SDSS galaxies with masses $> 10^{10} M_\odot$ (Panter et al. 2008; Gallazzi et al. 2006). Each method uses different stellar continuum wavelength ranges and features, and thus the discrepancy may reflect a real difference in the metallicity of stars contributing most light to the bluer wavelengths, or a small inconsistency in the stellar population synthesis mod-

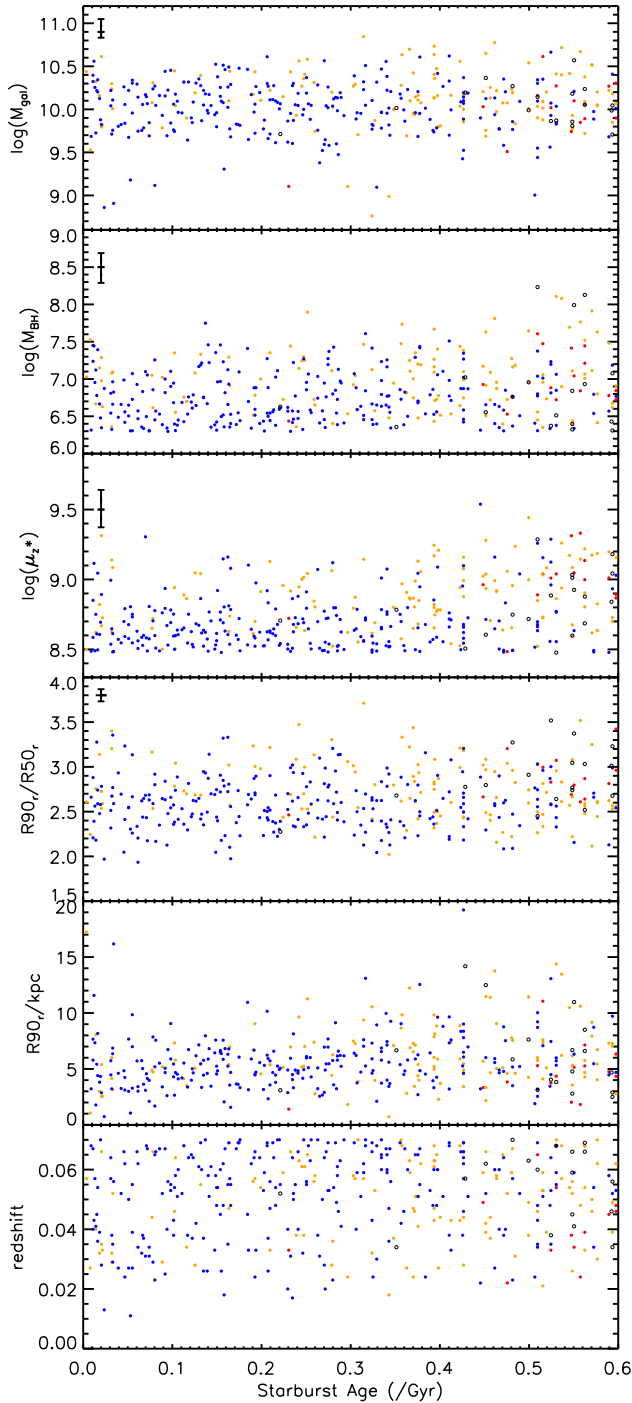


Figure 2. Trends of key galaxy properties with starburst age. In all panels, blue points indicate star-forming galaxies, orange indicate star-forming-AGN composites, red indicate pure AGN and black open circles are unclassified due to having too weak lines. Typical errors are noted in the upper left of each panel where significant. From top to bottom as a function of time since the onset of the starburst: (i) total galaxy stellar masses, calculated from the photometry and mass-to-light ratio taken from the likelihood distribution of the starburst models described in Section 2.2; (ii) black hole masses, measured from stellar velocity dispersion and assuming the $M-\sigma$ relation (Tremaine et al. 2002); (iii) stellar mass surface density, measured from the total stellar mass and the Petrosian half light radius in the z -band; (iv) concentration index, measured from the r -band Petrosian radii which enclose 50 and 90% of the light; (v) physical size, measured from the r -band Petrosian radius which encloses 90% of the light; (vi) redshift.

elling. Bursts of star formation with exponentially declining star formation rates ($\text{SFR} \propto \exp(-t/\tau)$) are superposed on this old stellar population, allowing burst mass fraction, burst age, decay rate and dust to vary with uniform priors. Burst age is allowed to range from 0 to 1.5 Gyr, burst mass fraction from 0 to 50% and dust (τ_V) from 0 to 2. While the decline in star formation subsequent to a starburst is not constrained from the integrated spectrum of an individual galaxy, the entire distribution of continuum spectral indices observed in galaxies does provide some additional constraint. For a model in which star formation rate declines exponentially, τ values much greater than 0.3 Gyr are excluded as they would not produce the observed population of post-starburst galaxies (Wild et al. 2009). Very short values of τ are equally excluded, because a burst that is strong enough to reproduce the starburst galaxies with short τ , evolves along a track which lies to the left of the observed edge of the distribution in Fig. 1, where no galaxies are observed. Requiring consistency between the decay in $\text{H}\alpha$ luminosities, which probe instantaneous star formation rates, and the age estimated from the continuum provides an additional constraint. Finally, we allow exponentially declining starbursts with $200 < \tau/\text{Myr} < 350$. We note that this starburst timescale is considerably longer than the “instantaneous” starbursts often assumed in the literature when measuring the ages of stellar populations in starburst and post-starburst galaxies. Our longer decay timescales result in slightly older derived ages, and may explain the population of galaxies with both strong Balmer absorption and emission lines (so-called e(a) galaxies)¹.

For each galaxy, the age of the starburst is estimated from the mode of the probability distribution function of model ages in the standard way. Starburst ages are well constrained, distributions are unimodal until beyond the maximum age presented in this paper, and ages are not sensitive to priors or dust reddening effects of the stellar continuum. Precise starburst mass fractions for individual objects are less well constrained than starburst ages. Rather than relying on estimated burst mass fractions to define our sample of the strongest starburst galaxies, we select a constant number of galaxies with the lowest 4000\AA break strength at each starburst age. As described above, the total number of starbursts selected for the strong-starburst track sample trades completeness at late ages against sample statistics. At late ages, old/strong starbursts become degenerate with younger/weaker starbursts. Selecting 20 starbursts per 30 Myr time bins gives a statistically adequate total sample of 400 galaxies complete to 600 Myr without risking the inclusion of galaxies at later times which are in fact younger, weaker starbursts. 600 Myr is long compared to the expected timescale of AGN accretion events (10^7 to 10^8 years), and our results present “volume-averaged” quantities, averaging over a large enough sample of galaxies to smooth out the stochastic nature of AGN activity.

2.3 Summary of sample properties

To summarise our selection criteria:

- Our base catalog is drawn from the SDSS DR7 spectroscopic catalog of spectroscopically identified galaxies with extinction corrected r -band Petrosian magnitude $14.5 < r < 17.7$.

¹ More complicated star formation histories, such as those with an initial slow decline and fast later decline, could also produce the observed population of post-starburst galaxies. However, this would only result in a small overall stretching/contracting of the starburst age axis in places.

- We isolate galaxies with bulges based on their stellar surface mass densities $\mu^* > 3 \times 10^8 M_\odot/\text{kpc}^2$.
- Our sample is limited to $0.01 < z < 0.07$ to ensure the spectrum observed through the $3'$ fibre aperture is dominated by the light from the bulge.
- Due to the velocity resolution of SDSS spectra, we only accept galaxies with stellar velocity dispersion, measured within the fibre, of $> 70\text{km/s}$.
- From this base catalog, we select the 400 bulges undergoing the strongest central starbursts, with starburst age $< 600\text{Myr}$. This sample is complete in the sense that we select an equal number of starbursts per unit age.

The starburst sample is shown as coloured dots in Fig. 1, the smoothness of the line traced by its right-hand edge is impressive and supports our interpretation of the distribution of the spectral indices. The stellar masses, black hole masses, stellar mass densities, concentration indices, sizes and redshifts of galaxies in our starburst sample are shown in Fig. 2 as a function of starburst age. In Appendix A we present two panels of images of the youngest and oldest starbursts in our sample. Note in particular the size of the SDSS fibre through which the spectrum is taken indicated in the top left of the Fig. A1.

The total stellar masses of the galaxies presented in Fig. 2 range typically between 5×10^9 and $5 \times 10^{10} M_\odot$. These masses have been estimated from the probability distribution function of mass-to-light ratios output from the models described above, and are consistent with those determined independently from SDSS fibre magnitudes. Based on these model fits, our sample of starburst galaxies have converted a mass of gas into stars that is typically around 10-15 percent of the total stellar mass of stars in the fiber aperture. Because starburst mass fractions derived from stellar continua are slightly prior dependent, we also estimate burst masses from the $H\alpha$ luminosities of the galaxies (presented in the following section). These suggest a slightly higher typical burst mass fraction of 25 percent.

3 BLACK HOLE ACCRETION RATE

We are interested in two quantities that describe the growth of the black hole. Firstly, the black hole accretion rate (BHAR, dM_{acc}/dt) that we estimate directly from the extinction corrected [O III] line luminosity using a bolometric correction of 600, which corresponds to the conversion $\text{BHAR}/(M_\odot/\text{yr}) = 4 \times 10^{-10} L_{\text{OIII}}/L_\odot$. Secondly, the black hole growth rate ($dM_{\text{acc}}/dt/M_{\text{BH}}$) which characterises the timescale for the black hole to double its mass, and which we quote in units of the Eddington Luminosity² (L_{Edd}), assuming a radiative efficiency of accretion of 10%. The distinction between BHAR as measured by L_{OIII} , and black hole growth rate as measured by $L_{\text{OIII}}/L_{\text{Edd}}$ can be confusing. Throughout the paper we refer to these quantities as “accretion rate” and “growth rate” respectively.

In order to measure “growth rates” we estimate the black hole masses from the stellar velocity dispersion of the galaxies (σ) by assuming the empirically calibrated $M_{\text{BH}} - \sigma$ relation (Tremaine et al. 2002). We note that elliptical galaxies, classical bulges (bulges in galaxies with disks) and pseudo-bulges follow

slightly different $\sigma - M_{\text{bulge}}$ relations, and therefore M_{BH} estimated from a $M_{\text{BH}} - \sigma$ relation will be different from that estimated from a $M_{\text{BH}} - M_{\text{bulge}}$ relation (Hu 2008; Gadotti & Kauffmann 2009; Graham & Li 2009). The offset can be attributed primarily to the presence of bars. However, as our results are based upon an average over a large sample of AGN, we do not believe this will introduce large biases. It is possible that bars are more prevalent in the youngest starbursts, in which case this effect will lead to slightly enhanced black hole mass estimates. We will note the implications of this effect where necessary in the results and discussions sections.

We separate our starburst galaxies into those with and without obscured AGN using optical emission line ratios (Baldwin et al. 1981; Kauffmann et al. 2003; Kewley et al. 2006). For galaxies with a contribution to their emission lines from both star formation and AGN (“composite AGN” - the majority of AGN in our sample) we have removed the contribution to [O III] from star formation using an empirically calibrated mixing algorithm. In the following subsections we give further details of these procedures. Firstly, we justify the use of [O III] as an indicator of black hole accretion rate.

3.1 [O III] as a black hole accretion rate indicator

For obscured (Type 2) AGN observed in the optical wavelength range the high ionisation [O III] $\lambda 5007$ emission line is the best available measure of AGN power. The luminosity of this line, which originates in the Narrow Line Region, has been shown to correlate with numerous indicators of total AGN power in unobscured (Type 1) samples, where the central engine can be viewed directly to obtain bolometric luminosities (e.g. Mulchaey et al. 1994). For obscured (Type 2) AGN, [O III] luminosity correlates well with hard X-ray luminosity for Compton thin AGN, with a scatter of 0.51dex over 4 orders of magnitude in luminosity (Heckman et al. 2005). Furthermore, because the AGN Narrow Line Region lies 100's of parsecs from the central engine, [O III] is not affected by dust obscuration from the torus, unlike X-ray emission which can be heavily absorbed (Compton thick AGN).

The conversion of [O III] luminosity into a bolometric AGN luminosity, from which we estimate black hole accretion rates, is based on the strong linear correlation between narrow [O III] emission and optical continuum luminosity in unobscured AGN (Zakamska et al. 2003). The conversion is discussed in detail in Heckman et al. (2004) and Kauffmann & Heckman (2009). However, we note here the implicit assumptions in this conversion for completeness. Firstly, the conversion is necessarily calibrated on unobscured AGN. By assuming this calibration holds for obscured AGN, we assume the AGN standard model in which [O III] is isotropically emitted and the difference between obscured and unobscured AGN is in the orientation of the dusty torus relative to our sightline. Secondly, SDSS AGN samples extend to lower luminosities than the samples used for the calibration. However, as shown by Heckman et al. (2004) and discussed below, the total [O III] luminosity of a volume limited sample of AGN is dominated by AGN with high [O III] luminosities. Removing galaxies with [O III] luminosities below the limit to which the conversion has been verified has little effect on volume averaged total black hole accretion rates. Finally, it should be noted that at some level L_{OIII} should depend on the availability of gas clouds to ionise, and may therefore correlate with host galaxy properties. This may plausibly account for some of the scatter in the observed relations between L_{OIII} and other indicators of AGN strength. We do not believe it is likely that there is a substantial increase in the number of narrow line clouds

² $L_{\text{Edd}}/L_\odot = 3.3 \times 10^4 M_{\text{BH}}/M_\odot$ is the luminosity at which radiation pressure due to electron scattering balances the inward pull of gravity for optically thin spherical accretion onto the black hole.

over timescales of several hundred Myrs, which could mimic the results found in this paper, especially given the relatively slow decline in star formation which presumably originates from the same gas supply.

3.2 Missing lower luminosity and unobscured AGN

There are two main ways in which the SDSS narrow line AGN sample is an incomplete census of the local AGN population: (1) loss of low luminosity/low growth rate AGN when the lines become indistinguishable from nebular emission from H II regions, or against the background stellar light; (2) broad line (unobscured) AGN are not included, because the bright nuclear light would preclude studies of the integrated galaxy stellar light.

Obscured, low luminosity AGN constitute the majority of the low- z AGN population (Hao et al. 2005), and recent deep X-ray surveys of local galaxies are revealing increasingly high fractions of low accretion rate AGN (Gallo et al. 2008). Hard X-ray observations are the most sensitive probe for (Compton thin) obscured AGN, and such low accretion rate systems would not be detected against the background stellar light in SDSS spectra. But, although these ultra low luminosity AGN are numerous, as noted above their contribution to the volume averaged growth of black holes is small (Heckman et al. 2004).

The volume averaged growth of black holes is dominated by high growth rate (L/L_{Edd}) systems (see discussion in Hao et al. 2005). More specifically, Heckman et al. (2004) find that the low- z volume averaged black hole growth rate peaks for black holes with masses of $\sim 10^{7.5} M_{\odot}$ (their Fig. 1) and is dominated by systems with $L/L_{\text{Edd}} \gtrsim$ a few percent (their Fig. 3). Therefore, while missing low-luminosity obscured AGN will have a negligible effect on estimated global BHARs, we may legitimately be concerned about missing high-luminosity unobscured AGN. Although the standard model for AGN suggests we can simply scale our results by the observed ratio of unobscured to obscured AGN, deviations from this model may affect our conclusions. We will return to this point where necessary in the discussion.

3.3 Emission line analysis

Emission line fluxes and errors, corrected for stellar continuum absorption, are extracted from the SDSS-MPA catalog (<http://www.mpa-garching.mpg.de/SDSS/>), see Brinchman et al. (2004) and Tremonti et al. (2004) for details of their measurement. All lines are corrected for dust attenuation using the observed $H\alpha$ to $H\beta$ ratio and the two component dust attenuation curve of Charlot & Fall (2000), as presented in Wild et al. (2007) and de Cunha et al. (2008). For star forming galaxies and composite-AGN (where emission from both star formation and an AGN is present), an intrinsic $H\alpha/H\beta$ ratio of 2.87 is assumed; for pure-AGN we use a slightly higher $H\alpha/H\beta = 3.1$ (Osterbrock 1989; Kewley et al. 2006). A very small fraction of our starburst galaxies have lines that are too weak to be measured accurately, about 4% of the starburst sample with ages younger than 600 Myr and 0.5% younger than 250 Myr. These fractions are too low to cause any bias in our results.

In Fig. 3 we present the $[\text{N II}]\lambda 6585/\text{H}\alpha$ vs. $[\text{O III}]/\text{H}\beta$ line ratio diagram (the BPT diagram, Baldwin et al. 1981) for all galaxies in our sample with lines measured at $> 3\sigma$ confidence. This diagram is commonly used to separate purely star forming galaxies from AGN (e.g. Kewley et al. 2001; Kauffmann et al. 2003). The

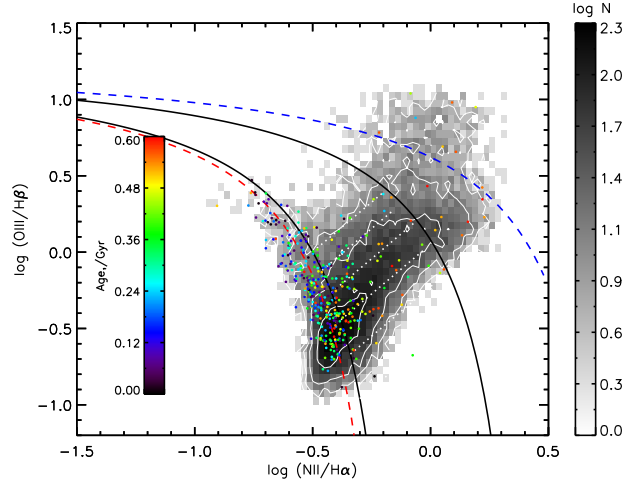


Figure 3. The BPT diagram. Bulge-galaxies with all four emission lines measured at $> 3\sigma$ are shown as gray-scale. The coloured circles are the starburst sample, with colour indicating starburst age as in Fig. 1. The lines indicate the positions of the demarcation lines C_{SF} (dashed red), C_{AGN} (dashed blue), $C_{\text{SF}/\text{comp}}$ (lower black) and $C_{\text{comp}/\text{AGN}}$ (upper black) as described in the text. The white dotted lines show how we assign κ to composite-AGN when the AGN and starforming contributions to the emission lines are calculated (Eqn. 5).

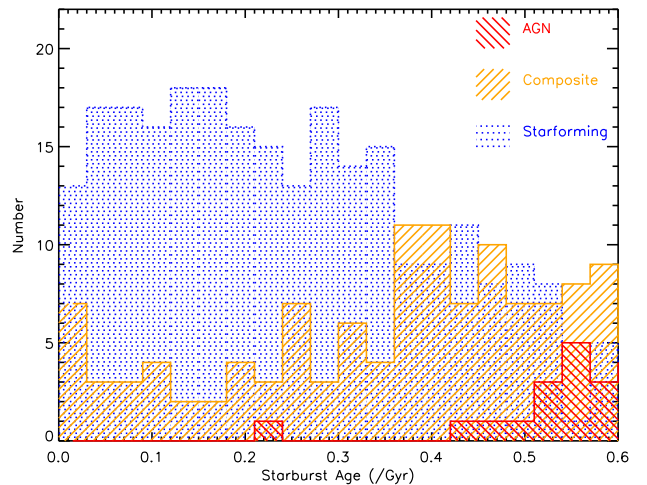


Figure 4. An important consequence of our results for the study of the AGN-starburst connection in individual objects using wide aperture integrated optical spectra alone, is that “pure” AGN will not be found in starburst galaxies, but only appear after the starburst. Before this time the star-formation will cause AGN to manifest as composite galaxies. Here we show the number of starforming (blue), composite-AGN (orange) and pure-AGN (red) in our sample as a function of time since the onset of the starburst.

starburst sample is overplotted, with colour indicating starburst age. We note that the trend for the youngest starbursts to have lower metallicities evident in this Figure is expected based on previous studies and simulations (Kewley, Geller & Barton 2006; Rupke, Kewley & Barnes 2010).

The upper black line lies close to the theoretical “maximum starburst” contribution from Kewley et al. (2001), above which Seyferts (high $[\text{O III}]/\text{H}\beta$) and LINERS (low $[\text{O III}]/\text{H}\beta$) are eas-

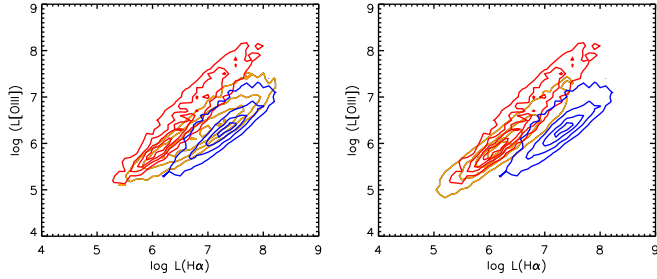


Figure 5. For composite-AGN we must separate the contributions to [O III] and H α emission from AGN and star formation. On the left is the distribution of total [O III] vs. H α luminosities for AGN (red), star forming galaxies (blue) and composite-AGN (orange). From outside to inside the contours encompass 90, 60, 30 and 10% of the data points. On the right, [O III] and H α luminosities for the composite-AGN have had the contribution from star formation removed as described in the text. We see that this correction procedure places the composite-AGN in the same range of [O III] luminosities as the pure AGN.

ily identified as plumes. As shown by Kauffmann et al. (2003) the ordinary star forming galaxies in the SDSS define a tight sequence that lies far below the theoretical model maximum, close to the red-dashed line indicated in the Figure. The simplest interpretation of the objects which lie between these two populations is that both starformation and AGN contribute to their emission lines, so-called “composite AGN”. This is supported by their younger ages as measured from the stellar continuum. The black lines indicate our separation between pure star forming galaxies and composite AGN (lower black line), and composite AGN and pure AGN (upper black line). The blue-dashed line is placed to cross through the center of the pure-AGN. The red-dashed line is placed to cross through the center of the star-forming galaxies

In this work, all demarcation lines are defined using the same equation for simplicity:

$$\text{BPT}_y = 1.3 + \frac{0.61}{\text{BPT}_x - C} \quad (1)$$

where the four lines in Fig. 3 are defined by $C_{\text{SF}} = -0.08$ (red), $C_{\text{SF}/\text{comp}} = -0.03$ (lower black), $C_{\text{comp}/\text{AGN}} = 0.5$ (upper black), and $C_{\text{AGN}} = 0.9$ (blue). We place the star-forming/composite demarcation line a little lower than that used by Kauffmann et al. for their sample. We will discuss the implications of the placement of this line on our results in the next subsection.

Galaxies which lie below $C_{\text{SF}/\text{comp}}$ have negligible contribution to their [O III] line from an AGN and we classify them as star forming galaxies, and those that lie above $C_{\text{comp}/\text{AGN}}$ have negligible contribution from star formation and we classify them as pure-AGN. Those that lie in between these two lines we classify as composite AGN. In Fig. 4 we plot the number of each emission line class vs. the age of the starburst, from which it is clear that in optical spectra probing a large spatial area pure-AGN will only be observed about 500 Myr after the onset of the starburst due to contamination of the AGN lines by the strong nebula emission from star formation. Before this time, AGN will necessarily be classified as “composite-AGN”.

In this paper, we include both composite and pure AGN in our measurements of the total BHAR and distributions of L/L_{Edd} . While galaxies which lie below the $C_{\text{SF}/\text{comp}}$ demarcation line may contain AGN, these will have very low L/L_{Edd} , therefore this line should be thought of as a limit on L/L_{Edd} of our AGN sam-

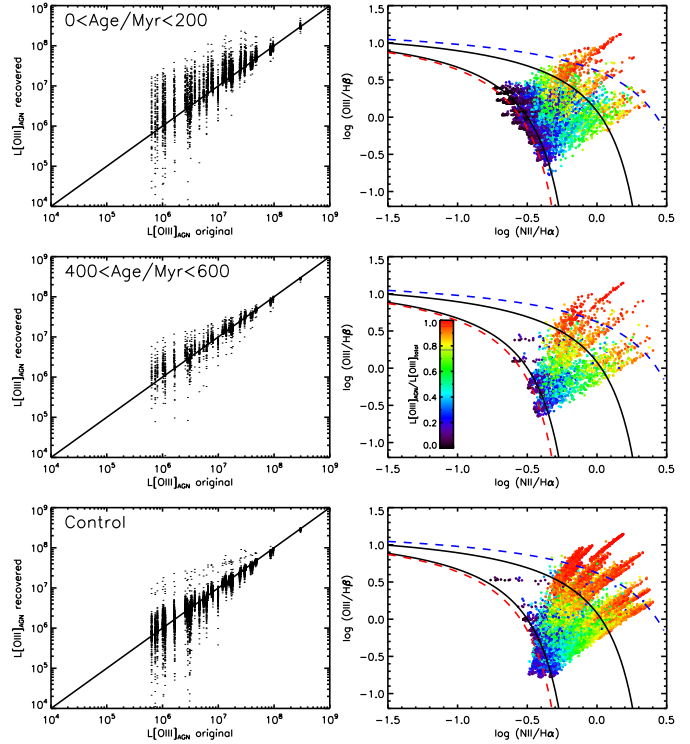


Figure 6. In the left panels we show the AGN contribution to L_{OIII} recovered from our Monte Carlo simulations combining AGN and star-formation-dominated galaxies using the correction method described in the text, compared to the true AGN L_{OIII} , for two different ranges of starburst age. In the right panels, we show the position of all the simulated composite-AGN on the BPT diagram, with the same demarcation lines as shown in Fig. 3. The points are colour coded by the AGN contribution to the total L_{OIII} of the simulation galaxy.

ple, rather than a firm division between galaxies with and without an accreting black hole (see also the detailed discussion in Kauffmann & Heckman 2009). We will return to this point later when we account for the incompleteness of our AGN sample as a function of L/L_{Edd} .

3.3.1 Correction of L_{OIII} for contamination from star formation in composite AGN

In order to measure the AGN luminosity of composite AGN from the [O III] emission line, we must correct for contamination due to starformation. Likewise, to measure star formation rates from H α luminosities, we must correct for contamination from the AGN. Our method is based upon the assumption that as AGN contribution increases, galaxies move diagonally away from the starforming sequence approaching the AGN demarcation line (following the white dotted lines in Fig. 3).

Inverting Eqn. 1 to obtain C for an individual composite AGN, we measure its distance from the starforming sequence to be:

$$D_{\text{BPT}} = \frac{C - C_{\text{SF}}}{C_{\text{AGN}} - C_{\text{SF}}} \quad (2)$$

which is normalised such that galaxies that lie in the center of the star-formation-dominated bulges (red dashed line) and in the center of the AGN-dominated bulges (blue dashed line) have $D_{\text{BPT}} = 0$ and $D_{\text{BPT}} = 1$ respectively.

Observing that both pure AGN and star forming galaxies in

our sample show very tight relations between $H\alpha$ and $[O\ III]$ luminosities (Fig. 5, left panel), and making the assumption that D_{BPT} defined in this manner is proportional to the fraction of $H\alpha$ luminosity arising from the AGN, we derive empirically the following correction for $[O\ III]$ and $H\alpha$ in the composite AGN:

$$L_{\text{OIII,AGN}} = L_{\text{OIII,Tot}} - \kappa(1 - D_{\text{BPT}})L_{\text{H}\alpha,\text{Tot}} \quad (3)$$

$$L_{\text{H}\alpha,\text{SF}} = L_{\text{H}\alpha,\text{Tot}} - D_{\text{BPT}}L_{\text{H}\alpha,\text{Tot}} \quad (4)$$

where Tot indicates the total contribution to the emission luminosity from both AGN and star formation. κ is the $[O\ III]/H\alpha$ ratio of starforming galaxies at the point on the starforming sequence where the composite AGN originated from (following the dashed white lines to meet the red dashed line in Fig. 3)

$$\log_{10}(2.87\kappa) = BPT_y^{SF} \quad (5)$$

$$= 1.3 + \frac{0.61}{BPT_x^{SF} - C_{SF}} \quad (6)$$

$$= BPT_y + m(BPT_x^{SF} - BPT_x) \quad (7)$$

which we solve numerically, setting $m = 1.3$ and assuming an intrinsic $H\alpha$ to $H\beta$ flux ratio of 2.87 (Osterbrock 1989). The success of the separation procedure can be seen in the right panel of Fig. 5 where the corrected $[O\ III]$ to $H\alpha$ line luminosities of the composite-AGN follow the relation of the AGN.

3.3.2 Monte Carlo simulations of the L_{OIII} correction procedure

Because the correction of L_{OIII} for contamination from star formation is not yet common practice in the literature, and has not been thoroughly tested, we present here a simulation to demonstrate the validity of the technique. We proceed by taking all pure-AGN with starburst ages $> 250\text{Myr}$, and add their lines one-by-one into each pure star forming galaxy in our starburst sample. We do this for different age bins of the star-formation-dominated starburst galaxies and repeat the experiment for a control sample of blue-sequence bulge-galaxies. This control sample is extracted from the region defined by the dotted box in Fig. 1 and is matched to the starburst sample in black hole mass, stellar mass, redshift and stellar surface mass density. We then recalculate the position of the galaxies on the BPT diagram, perform our $[O\ III]$ separation analysis and compare the output AGN component of the total $[O\ III]$ luminosity, to the input true AGN luminosity.

The result is shown in Fig. 6 for two starburst samples with age bins of $0 < \text{age}/\text{Myr} < 200$ and $400 < \text{age}/\text{Myr} < 600$, and the control sample of blue-sequence bulge-galaxies. Similar results are obtained for the intermediate age starburst sample. The left hand panels show that on average we recover the input L_{OIII} well. The right hand panels show the simulated composite-AGN on the BPT diagram, colour coded by the fraction of L_{OIII} contributed by the AGN. On average we see that, as expected, galaxies close to the SF-composite demarcation line (lower black line) have small contributions, whereas those that sit close to the composite-AGN demarcation line (upper black line) have contributions close to unity.

It is noticeable that the youngest starbursts suffer from an overestimation of $L_{\text{OIII,AGN}}$ by about a factor of 2 on average. This results from their lower mean metallicity which, if mixed with a LINER ratio AGN, means they do not follow the assumed mixing tracks on the BPT diagram. When mixed with Seyfert line ratios, however, the method works accurately. We emphasise that the method presented here is suitable for the majority of bulge-dominated galaxies at low-redshift. However, for low-metallicity

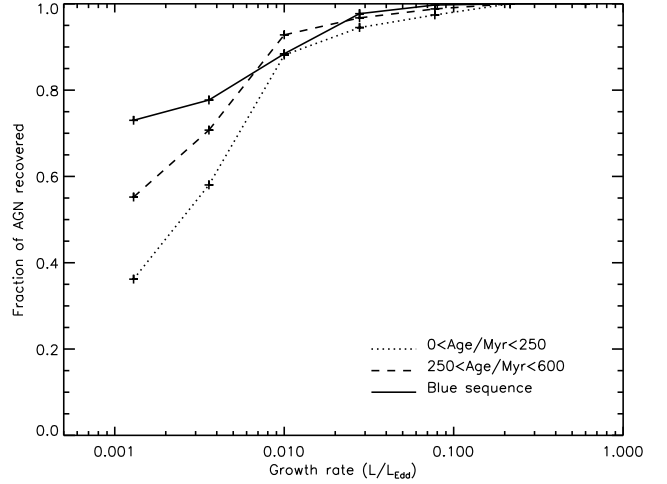


Figure 7. Result of the Monte Carlo simulation to estimate the fraction of AGN recovered as a function of normalised BHAR (L/L_{Edd}) and starburst age. The dotted and dashed lines are for the starburst sample with ages as indicated in the figure. The solid line shows the result for the control sample of ordinary bulge dominated starforming galaxies. By 250 Myr after the starburst, the fraction of AGN recovered is similar to the control sample, however, at younger ages we can recover fewer AGN due to the masking of AGN lines by the emission lines from starforming regions. In our analysis we only include bins which are $>50\%$ complete.

star-forming regions there is ultimately a degeneracy that prevents a unique solution for the fraction of L_{OIII} originating from the AGN using these line ratios alone. In Section 4 we deliberately exclude the very youngest starbursts ($< 30\text{Myr}$) from some parts of our analysis, which reduces the impact of this degeneracy as these galaxies have the lowest metallicities (see Fig. 3 and Section 3.3). We note in the results and discussion sections where this may affect our results.

3.4 AGN Completeness

There are three possible causes for not identifying AGN in a purely optical sample: (1) the AGN emission lines are completely concealed by the strong nebular lines from star formation; (2) the AGN emission lines are not identifiable against strong stellar continuum radiation; (3) the AGN emission lines are obscured by dust. For the results presented in this work, we are primarily concerned about correcting for the first effect, which causes us to preferentially lose weaker AGN in the youngest starbursts. Effect (2) will not cause a similar bias as the red broad-band magnitudes of the sample change little with the time probed and the low AGN luminosities involved do not contribute significantly to the time averaged BHAR as discussed in Section 3.1. Effect (3) may cause us to lose a small number of objects at older ages ($> 350\text{Myr}$) corresponding to the onset of the Asymptotic Giant Branch phase in lower mass stars, where we start to see a significant increase in the mean Balmer decrement of the starburst galaxies. This trend of dust content with starburst age is the subject of future work.

Returning to the first effect, we use the simulations described above to calculate the completeness of our samples as a function of L/L_{Edd} by calculating the position of the simulated composite AGN on the BPT diagram and finding whether they would be included in our AGN sample or not (i.e. lie above the lower black line

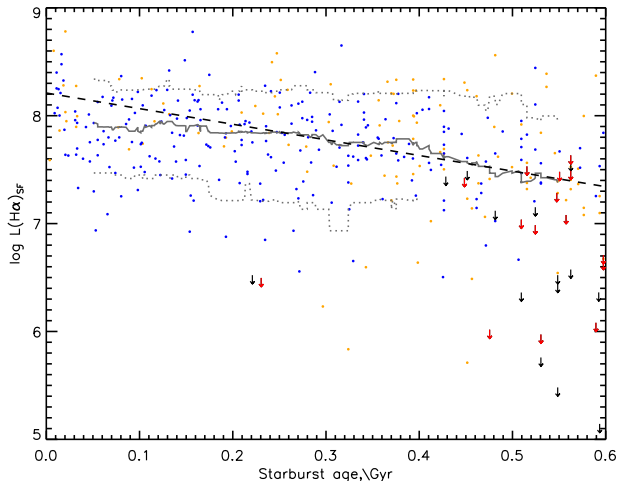


Figure 8. $H\alpha$ luminosity from star formation, corrected for dust attenuation and contamination from AGN emission as described in the text. Blue points indicate star-forming galaxies, orange indicate star-forming-AGN composites. Upper limits indicate unclassified objects (black) and pure-AGN (red). The gray solid line and dotted gray lines trace the 50th, 10th and 90th percentiles of the distribution using a running bin width of 71 galaxies. The black dashed line shows an exponentially declining star formation rate with $\tau = 0.3$ Gyr, normalised to the median SFR in the first 40 Myr. Due to the significant fraction of objects at late ages for which we only have upper limits of $L(H\alpha)$ the 10th percentile is only indicated to 400 Myr.

in Fig. 3). The resulting measured completenesses, shown in Fig. 7, are then included in all quoted values of the AGN fraction. We can see that even at the youngest starburst ages we recover $>90\%$ of AGN with $L/L_{\text{Edd}} > 0.01$, and at later times this rises to 95%. Therefore, we are not losing a significant number of high accretion rate AGN from our samples. However, it is clear that AGN with $L/L_{\text{Edd}} < 0.003$ are difficult to detect at all ages during the starburst, with recovery rates of $<50\%$. In order to investigate further the appearance of low accretion rate AGN, follow-up observations at higher spatial resolution and, possibly, in other wavebands will be necessary.

In order to be sure that our key results are completely robust to changes in the precise positioning of the demarcation between star forming galaxies and AGN (lower black line in Fig. 3), we repeat the key results but this time allowing all galaxies which lie above the red line in Fig. 3 to be composite-AGN. We find that although, of course, there are many more “AGN” in our sample these have low growth rates and the total BHAR remains the same.

3.5 Decline in SFR of a starburst

Not only does our starburst sample allow us to investigate the time averaged AGN activity during a starburst, as presented in the results section below, it also provides a means by which to measure the form of the decay in star formation after the onset of a starburst. Very few constraints currently exist on this decay timescale, and instantaneous or very short starbursts are often assumed in the literature which are not consistent with the results presented here.

In Fig. 8 we present the $H\alpha$ luminosity of all starforming and composite galaxies in our starburst sample, as a function of starburst age derived from the stellar continuum. Composite galaxies have had the contribution to $H\alpha$ luminosity from AGN removed (Eqn. 4). We can clearly identify 3 phases: a short “starburst” phase

of order 10-30 Myr, an almost flat “coasting” phase which lasts to around 400 Myr, and a subsequent decline. Throughout this paper, we have parameterised the overall decline in starformation by an exponential. In this Figure an exponential with a timescale of $\tau = 0.3$ Gyr is overplotted as a black dashed line. It is normalised to the median $H\alpha$ luminosity in the first 40 Myr. As discussed in Section 2.2, when fitting starburst ages to our bulge-galaxies we assume a range of τ values for the starburst models. This range was decided upon by taking the observed decline in $H\alpha$ luminosities into account: allowing τ values much shorter (longer) causes the observed $H\alpha$ luminosities of the older starbursts to lie above (below) the predictions of the models used to estimate the starburst age. While neither stellar continuum nor line luminosities alone constrain the fall in star formation during a starburst, it is encouraging that a simple model shows that they can be consistent with each other. A more precise study of the decline in star formation following a starburst will be feasible with the data and methods presented here.

The starburst timescales of several hundred Myrs measured here are consistent with measurements from two entirely independent methods. Firstly, from observing starbursts in close galaxy pairs (Barton, Geller, & Kenyon 2000; Freedman Woods et al. 2010), and secondly from the stellar mass surface density profiles of elliptical galaxies (Hopkins & Hernquist 2009). In the latter paper a very similar form for the star formation history is also inferred for the component of elliptical galaxies thought to be formed during gas rich starbursts.

4 RESULTS

By averaging over a sample of 400 bulge-galaxies, we can build a picture of the time-averaged BHAR with respect to the global star formation activity of the sample, even though individual accretion events may be relatively short lived. To calculate the average black hole accretion rate occurring in each time bin, we sum the total L_{OIII} originating from the pure- and composite-AGN corrected for contamination from star formation, and divide by the total number of starburst galaxies in that bin, i.e. including the pure starbursts currently not experiencing a strong black hole accretion event. In the top panel of Fig. 9 we plot the mean BHAR ($M_{\odot}/\text{yr}/\text{galaxy}$) as a function of time since the onset of the starburst, finding it to remain low during the early phase of the starburst, and increase only at ages >250 Myr. A similar offset between starburst and AGN activity has been suggested for a handful of nearby galaxies studied in detail (e.g. Tadhunter et al. 1996; Emonts et al. 2006; Goto 2006; Davies et al. 2007). In the lower panel of Fig. 9 we show how the ratio of SFR/BHAR evolves rapidly with time since the starburst, where SFR is measured directly from $H\alpha$ luminosity. We find that the total mass of stars formed is 2×10^3 times the total mass accreted onto the black hole during the first 600 Myr after the starburst. This ratio is a little higher than, but of the same order as the ratio of stellar mass to black hole mass in present-day bulges (Haring & Rix 2004), suggesting that the processes we observe in the starbursting bulges may be more broadly relevant to the co-evolution of bulges and black holes. We will return to this point in the discussion. We have deliberately not plotted the average BHAR for starbursts with ages younger than 30 Myr in Fig. 9 (20 galaxies), because of the additional incompleteness for these galaxies with extreme star formation rates and the additional uncertainty in the separation of [O III] into starformation and AGN components (i.e. the initial spike of galaxies with strong $H\alpha$ fluxes in Fig. 8).

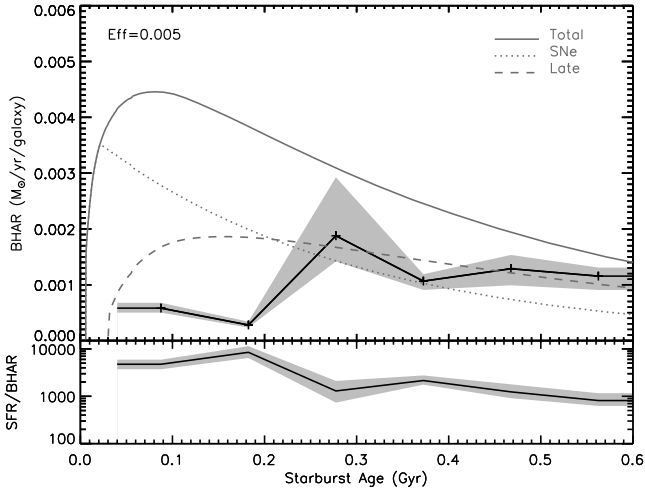


Figure 9. Top Panel - the mean BHAR averaged over all galaxies in the sample (black line), estimated from a robust mean with 5σ clipping. The gray shaded area shows the typical 10th and 90th percentile range on the total BHAR estimated from bootstrap resampling of the data. The initial 30 Myr after the onset of the starburst is not plotted, as explained in the text. The model prediction for the average gas mass loss rate from the stars formed during the starburst (solid gray line) assumes an accretion efficiency onto the black hole of 0.5% of the ejecta from low-mass stars between the age of 250 and 600 Myr. Stars return mass to the interstellar medium through SNe explosions and fast winds from massive stars (dotted line) and planetary nebula ejections and stellar winds from lower mass stars (dashed line). Bottom panel - the ratio of SFR (from H α) to BHAR, with mean value and errors calculated as for the top panel.

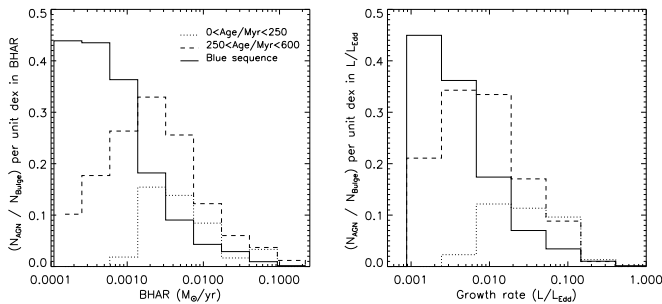


Figure 10. The AGN fraction in bulge-galaxies with starburst ages <250 Myr (dotted line), with starburst ages between 250 and 600 Myr (dashed line) and for bulges undergoing ordinary star formation and matched to the starburst sample in stellar mass, surface mass density, black hole mass and redshift (solid line, see dotted box in Fig. 1). *Left:* As a function of BHAR. *Right:* As a function of black hole growth rate (L/L_{Edd}). In both panels the AGN fractions have been corrected for incompleteness caused by the concealment of AGN emission by emission from star forming regions, and only bins which are >50% complete are plotted.

To uncover the primary factor driving the low global accretion at young starburst ages, in Fig. 10 we plot the distribution of BHAR (left) and growth rate (right) in the starburst and control samples. We have divided the starburst sample into two at 250 Myr and we compare to galaxies with more ordinary recent star formation histories (blue-sequence bulge-galaxies matched in black hole mass, stellar mass, redshift and stellar surface mass density, see dotted box in Fig. 1). All histograms have been corrected for incompleteness in the samples as a function of L/L_{Edd} and starburst age (Fig.

7 and Section 3.4) and only bins with an overall completeness of greater than 50% are plotted. Comparing the distribution of BHAR (left panel) in the three samples we see that both young and old starbursts show an enhanced number of powerful AGN with respect to the control blue-sequence sample, which has been matched to the starburst sample in redshift, stellar mass, stellar mass surface density and black hole mass. However, in the youngest starbursts the AGN fraction is reduced at all accretion rates relative to the AGN fraction in the older starbursts. In both young and old starburst samples the distribution of BHAR turns over at low BHAR, suggesting that low accretion rate AGN in starbursts are suppressed compared to in ordinary star forming bulges. However, given the increasing importance of completeness corrections at lower BHAR this result should be verified with additional observations.

The right hand panel of Fig. 10 provides a different view of black hole accretion patterns during the starburst. Here we see that the fraction of starbursts with rapidly growing black holes is enhanced relative to our control sample of blue-sequence bulge-galaxies. Specifically, the fraction of galaxies with black holes accreting at rates greater than 0.7% of the Eddington rate is ~ 1.2 times higher in starbursts with ages between 0 and 250 Myr, than in ordinary blue-sequence bulge-galaxies, and ~ 2 times higher in starbursts with ages between 250 and 600 Myr. Although incompleteness prevents us from probing to very low growth rates, the turn-over in the distribution of L/L_{Edd} occurs at higher L/L_{Edd} in the youngest starbursts, compared to both the older starbursts and the control sample. The shape of these distributions strongly suggest that low growth-rate accretion events are suppressed during the starburst.

We have not included the 7 composite-AGN with ages younger than 30 Myr in the dotted histograms of Fig. 10, for the reasons explained above. The effect of including them is small, and does not change the impression given by the figures. As discussed in Section 3, it is possible that the presence of bars at certain phases during the starburst may cause biases in the right panel of Fig. 10, due to our estimation of black hole mass from stellar velocity dispersion. However, the most likely consequence is that we slightly overestimate the black hole mass of a small fraction of galaxies with the youngest starburst ages. Correcting for this would only enhance our conclusion that the highest growth rate events are not suppressed in young starbursts.

Combining all these results we conclude that the global accretion onto black holes is lower in young starbursts than in older starbursts. This is caused by an overall drop by around a factor of two in the number of accretion events at all BHARs above at least $10^{-3} M_{\odot}/\text{yr}$. The possible trend for the turnover in the distribution of L/L_{Edd} to occur at higher values of L/L_{Edd} in starbursts compared to the control sample, and at higher values in younger compared to older starbursts, should help constrain the physical mechanism responsible for this decrease. We will return to this point in the discussion.

4.1 Summary of observational results

The existence of some connection between starbursts and AGN has been debated for several decades. Sanders et al. (1988) argue for an evolutionary connection on galaxy wide scales between ULIRGs and QSOs. Heckman et al. (1997) argue for a causal connection on nuclear scales (González Delgado et al. 2001; see Veilleux 2001 for a review of the subject). Here we argue for its existence for the first time based on a large statistical sample with a well defined control

sample. However, we modify the nature of connection in several ways. To summarise the key observational results, we find that:

- Galaxies with bulges experiencing a strong starburst are more likely to host a rapidly growing and rapidly accreting black hole than galaxies with bulges experiencing more normal levels of star formation.
- The total mass of stars formed in the first 600 Myr after the onset of the starburst is 2×10^3 times the total mass accreted onto the black hole. The black holes increase their mass by on-average 5% during this time.
- On average, the rate of accretion onto black holes rises steeply about 250 Myr after the onset of a burst of star formation.
- The lower average BHAR in young starbursts compared to old starbursts is caused by a decrease by about a factor of two in the number of accretion events at all BHARs above at least $10^3 M_\odot/\text{yr}$.
- Alternatively, our results can be viewed as an enhancement in the global accretion onto black holes during a starburst, relative to that occurring in ordinary blue-sequence bulge-galaxies, but mainly in bulges with starbursts older than 250 Myr.
- On the rare occasions that a black hole accretes during the early phase of the starburst, it grows rapidly (has $L/L_{\text{Edd}} > 0.01$).
- While higher growth rate events are enhanced compared to blue-sequence bulge-galaxies, lower growth rate events instead appear suppressed.

We note that our results apply primarily only to black holes in the mass range $10^{6.5} - 10^{7.5} M_\odot$, moderate luminosity AGN (bolometric luminosities of order $10^{42} - 10^{44}$ erg/s), and powerful starbursts which increase the stellar mass in the central $\lesssim 2$ kpc radius of the galaxy by at least 10%.

5 DISCUSSION

5.1 Unobscured AGN

To begin our discussion, we return to one of the assumptions implicit in our calculations: to extrapolate our results for obscured (Type 2) AGN to the growth of all black holes, the simplest approach is to assume the standard unified model for AGN in which the difference between unobscured and obscured AGN is in the viewing angle alone. Under this assumption, the effect of our exclusion of unobscured (Type 1) AGN will mean that we have undercounted the total amount of black hole growth in our population of starburst galaxies.

There have been many estimates of the ratio of Type 2 to Type 1 AGN in the local universe, with values ranging between ~ 3 (e.g. de Grijp et al. 1992) and ~ 1 (e.g. Hao et al. 2005). Thus, we would need to increase the rate of black hole accretion by factors ranging from 1.3 to 2. There is some dispute about whether the relative number of Type 1 and Type 2 AGN is an increasing function of luminosity at low redshift. For example, de Grijp & Miley (1992) found no evidence for such a dependence based on the mid-IR luminosity functions, while Hao et al. (2005) found that the ratio did increase by a factor of 2-4 over a range of about four orders of magnitude in [O III] luminosity. Thus, we may be underestimating the relative importance of high accretion rate events by examining only obscured AGN.

A more interesting possibility would be that the Type 1 and Type 2 AGN are related to one another in an evolutionary sense (and not distinguished purely by viewing angle). For example, it is physically plausible that obscured AGN evolve into unobscured

AGN as feedback associated with the AGN and/or the surrounding starburst clear away much of the obscuring material (e.g. Sanders et al. 1988). In this case, by excluding Type 1 AGN we may be selectively undercounting the relative amount of black hole growth during the late phases of the starburst compared to the early stages. If so, and if this scenario were applicable to the moderate luminosity AGN studied in this paper, then this would only increase the sense of the increase in black hole growth at these late times.

It is interesting in this regard that Davies et al. (2007) have measured the nuclear starburst ages of a sample of mostly unobscured local AGN, finding a time delay between the onset of the starburst and the onset of significant black hole accretion. The magnitude of the delay was similar, although a little shorter than, that found in our study. As pointed out by Davies et al. (2007), the Galactic center also fits into this picture, where the winds from nearby young OB stars are not being accreted as efficiently as expected (Baganoff et al. 2003; Paumard et al. 2006).

5.2 Black hole accretion from stellar mass loss

One popular hypothesis for the physical mechanism responsible for the feeding of black holes is through the accretion of matter ejected during stellar evolutionary processes (Norman & Scoville 1988). We can investigate the link between starburst activity and BHAR by examining the mass returned to the interstellar medium (ISM) by supernova (SNe) explosions, planetary nebula ejections and stellar winds predicted from standard stellar population synthesis models (Bruzual & Charlot 2003, Charlot & Bruzual, in prep.). The solid gray line in Fig. 9 shows the mass loss rate of stars formed during a starburst, and the dotted and dashed lines separate this into mass loss from high mass (predominantly SNe) and lower mass stars³. During the initial phase of the starburst mass loss from SNe explosions and fast winds from O/B stars dominates the mass loss budget, however as can be seen in Fig. 9, mass loss from lower mass stars soon becomes dominant. The model is normalised to match the total mass of gas per galaxy converted into stars in our starburst sample, which we have measured from the H α line luminosity, converted into star formation rate (Kennicutt 1998) and corrected for contamination from AGN. The star formation rate of the model declines exponentially with a timescale of 300 Myr, in agreement with the observed fall-off in the H α luminosity arising from star formation in the sample.

The model for stellar mass loss rate has been placed onto the same scale as the BHAR by assuming that 0.5% of the mass returned to the ISM by evolved low and intermediate mass stars within 250 and 600 Myr is accreted by the black hole. This fraction is similar to that predicted by, for example, the model of Ciotti & Ostriker (2007) and to that inferred in galaxy bulges with predominantly old stellar populations (Kauffmann & Heckman 2009). It is immediately evident that the average BHAR of the sample does not follow the *total* mass loss rate from stellar processes (solid line), in particular during the early period of rapid mass loss from SNe (dotted line). One key difference between mass loss from SNe compared to that from lower mass stars is in the ejecta velocity: several thousand km/s for SNe compared to several tens of km/s for lower mass stars. Fig. 9 suggests that the fast ejecta from SNe must escape the nuclear region without interacting with the central black hole.

³ Mass loss from low mass stars in the pre-existing old stellar population in the bulge is not significant during these phases of a strong starburst.

This is consistent with the model of Norman & Scoville (1988) and with detailed observations of nearby AGN (Davies et al. 2007).

If a simple model for the feeding of black holes through mass loss from *slow* stellar ejecta is correct, then an important question is whether SNe are simply inconsequential for black hole growth, or whether they cause enough disruption of the ISM to prevent the accretion of the slower stellar ejecta by the black hole. Two features of our results suggest that the latter may indeed be the case. Firstly, from Fig. 9 we see that the BHAR does not track the mass loss from intermediate and low mass stars at the earliest times between 100 and 200 Myr after the starburst. During this time, supernova rates remain high and may provide the energy required to inhibit the accretion of slower stellar ejecta and any residual gas. Secondly, in the right panel of Fig. 10 we see that the distribution of AGN fraction as a function of black hole growth rate changes with starburst age, i.e. while higher growth rate events are enhanced compared to blue-sequence bulge-galaxies, lower growth rate events are instead suppressed. This pattern is stronger in young starbursts than in old starbursts, and the turn-over in the distribution of L/L_{Edd} occurs at higher values for young starbursts than for old starbursts. A scenario in which growth rate is linked to the mass of an accreted cloud, and supernovae preferentially disrupt/expell the lowest mass clouds, would account for the observed suppression of low growth rate events during starbursts.

5.3 Alternative models for black hole accretion

Our observations have direct implications for theoretical models that attempt to explain the joint evolution of black holes and galaxies (Silk & Rees 1998; Haehnelt et al. 1998; Hopkins et al. 2006; Ciotti & Ostriker 2007). Our results clearly show that the rate of growth of the black hole is offset in time with respect to the *total* rate of stellar mass-loss. Moreover, the ratio of the mass accreted by the black hole to the mass lost by intermediate mass stars alone rises as the starburst ages. However, there are no direct observational constraints on the primary physical mechanism responsible for the feeding of a black hole. In the previous subsection we have chosen to focus our comparison on the scenario in which black holes feed primarily on stellar ejecta from intermediate-mass stars, due to its simple application to our data through stellar population synthesis modelling. However, we have found that this model in its simplest form is not sufficient to explain our results. A plausible additional component to the model, allowing it to match our results, is that supernovae disrupt the gas in the nuclear regions and prevent the early accretion of slower material ejected by lower mass stars. We now discuss two alternative scenarios which are not currently advanced enough to provide direct comparison with our data.

One alternative for the origin of the time delay is that stellar ejecta are initially intercepted by gas in the nucleus not yet converted into stars. Numerical simulations which could test this scenario are not yet available. A second possibility is that the delay in black hole growth could be purely dynamical in nature, relating to the collision of two bulges during a merger. Some of the images in Figs. A1 and A2 show galaxies which have experienced significant recent disruption. In simulations of major mergers with a black hole in each progenitor galaxy, rapid accretion occurs after coalescence of these black holes, which lags behind the peak of the starburst by a short time ($\sim 0.1\text{Gyr}$, e.g. Matteo et al. 2005; Johansson et al. 2009). Although this delay appears too short to match our results, higher spatial resolution simulations should be developed before this possibility is ruled out. Simulations are needed that better resolve the complex physical processes occurring in a galactic nu-

cleus during a starburst. Although both of these alternative scenarios for the feeding of black holes may plausibly lead to a delay in accretion after a starburst, the intriguing suppression of low growth rate accretion events during the starburst may still require the presence of some form of feedback process. In order to gather evidence for or against each of the scenarios discussed here, spatially resolved spectroscopy would be invaluable, allowing us to identify double nuclei, measure starformation rates as a function of radius, and obtain more accurate accretion rates.

Kauffmann & Heckman (2009) found that the distribution in the growth rates of black holes at low-redshift swaps from a power-law distribution for black holes in old bulges (little or no starformation) to a log-normal distribution for black holes in young star-forming bulges. They showed that the accretion rates in the old systems were consistent with the black hole accreting 0.3 to 1% of the mass loss from evolved stars in the bulge (consistent with the value we derive). They speculated that the transition to the log-normal regime was associated with the black hole regulating its own growth in the young gas-rich bulges. In this paper, we are suggesting that stars may not only provide the fuel source, but also the feedback (in the form of supernovae associated with actively star-forming bulges).

5.4 Implications for Starbursts

Our sample of starburst galaxies has other useful applications, besides tracing the growth of black holes, such as measuring the decay in star formation following a starburst (Section 3.5). It is clear both from these observational results, and from simulations of starbursts induced by mergers that the assumption of an exponential for the decay in star formation following a starburst is an oversimplification. Given the apparent complexities in star formation histories suggested by these simulations, it is perhaps surprising that our simple approach produces noticeable trends and easily interpretable results. With the development of galaxy simulations with higher spatial resolution, the inclusion of more realistic physical prescriptions of star formation, and the conversion of output into “observable” properties, in the near future we should be able to compare simulations directly with the sample presented in this paper to further constrain the true star formation histories of starbursts.

5.5 Global implications

Averaged over the full sample, we find that the black holes increase their mass by 5% during the first 600 Myr after the starburst. While clearly not the dominant phase of the growth of the black holes, this value is far from insignificant. We have purposefully restricted our sample to the strongest starbursts that occur in bulges in the local Universe, simply to enable an accurate measure of the star formation timescales. However, inspection of the images in Figs. A1 and A2 implies that our sample is not composed exclusively of rare major mergers, and the same time delay may equally apply to more ordinary episodes of star formation. At higher redshift, where gas fractions are higher, and star formation levels are enhanced, the same patterns observed in the strongest starburst systems at low redshift are expected to become more widespread. This would imply an increased fraction of high accretion rate AGN with redshift and, possibly, a decrease in the fraction of low accretion rate AGN. Growth rates would similarly be enhanced.

Over the lifetime of a galaxy the mass loss budget from stellar evolutionary processes is dominated by intermediate and low mass

stars, thus our results are consistent with a scenario in which the tight observed correlation between black hole and bulge mass is maintained through the consumption by the black hole of a fixed fraction of low-velocity winds expelled by such stars in the bulge.

To evaluate this quantitatively, we adopt a simple prescription in which we follow the evolution of the stellar mass loss and black hole growth over a period of 10 Gyr (the age of typical present-day bulges) in a model exponentially declining star formation history with decline timescale of 300 Myr. For simplicity, we assume that none of the supernovae ejecta are accreted by the black hole and that none (0.5%) of the low-velocity stellar ejecta are accreted before (after) a time of 250 Myr. The late-time accreted fraction we adopt is consistent with observations of black hole growth in old bulges (Kauffmann & Heckman 2009). This simple model predicts that at a time of 10 Gyr, the ratio of the remaining stellar mass to the accumulated black hole mass will be ~ 400 . Observations of present day bulges yield an actual mean ratio of 700 (Marconi & Hunt 2003; Häring & Rix 2004). Given the uncertainties in converting our measured [O III] luminosities into black hole accretion rates, uncertainties in the stellar mass-loss rates, and the simple model we have adopted, the similarity of these two values is quite intriguing. It suggests that the processes at work in our local starburst sample may well be relevant to the co-evolution of black holes and bulges over cosmic time, and that black hole growth has been fueled predominantly by mass loss from intermediate mass stars.

If stars are the primary source of fuel for growing the black hole and also play a major role in the feedback processes that limit this growth, then it starts to be less puzzling that black hole mass is linked to the stellar mass of the bulge.

ACKNOWLEDGEMENTS

VW gratefully acknowledges support from a Marie Curie Intra-European fellowship. We would like to thank in particular Dimitri Gadotti, Crystal Martin and Barnaby Rowe for helpful discussions. We acknowledge the anonymous referee for their useful comments which helped improve the manuscript. VW also acknowledges the astronomy groups at the University of Washington, UCSB, UCSC, Stanford and Caltech who all contributed useful feedback on this work when presented prior to publication.

Funding for the SDSS and SDSS-II has been provided by the Alfred P. Sloan Foundation, the Participating Institutions, the National Science Foundation, the U.S. Department of Energy, the National Aeronautics and Space Administration, the Japanese Monbukagakusho, the Max Planck Society, and the Higher Education Funding Council for England. The SDSS Web Site is <http://www.sdss.org/>. The SDSS is managed by the Astrophysical Research Consortium for the Participating Institutions. The Participating Institutions are the American Museum of Natural History, Astrophysical Institute Potsdam, University of Basel, University of Cambridge, Case Western Reserve University, University of Chicago, Drexel University, Fermilab, the Institute for Advanced Study, the Japan Participation Group, Johns Hopkins University, the Joint Institute for Nuclear Astrophysics, the Kavli Institute for Particle Astrophysics and Cosmology, the Korean Scientist Group, the Chinese Academy of Sciences (LAMOST), Los Alamos National Laboratory, the Max-Planck-Institute for Astronomy (MPIA), the Max-Planck-Institute for Astrophysics (MPA), New Mexico State University, Ohio State University, University of Pittsburgh, University of Portsmouth, Princeton University, the

United States Naval Observatory, and the University of Washington.

References

- Abazajian K. N., et al., 2009, *ApJS*, 182, 543
 Baganoff F. K., Maeda Y., Morris M., et al., 2003, *ApJ*, 591, 891
 Baldwin J. A., Phillips M. M., Terlevich R., 1981, *PASP*, 93, 5
 Barton E. J., Geller M. J., Kenyon S. J., 2000, *ApJ*, 530, 660
 Brinchmann J., Charlot S., White S. D. M., Tremonti C., Kauffmann G., Heckman T., Brinkmann J., 2004, *MNRAS*, 351, 1151
 Bruzual G., Charlot S., 2003, *MNRAS*, 344, 1000
 Cattaneo A., Faber S. M., Binney J., et al., 2009, *Nature*, 460, 213
 Charlot S., Fall S. M., 2000, *ApJ*, 539, 718
 Ciotti L., Ostriker J. P., 2007, *ApJ*, 665, 1038
 Couch W. J., Sharples R. M., 1987, *MNRAS*, 229, 423
 da Cunha E., Charlot S., Elbaz D., 2008, *MNRAS*, 388, 1595
 Davies R. I., Sánchez F. M., Genzel R., Tacconi L. J., Hicks E. K. S., Friedrich S., Sternberg A., 2007, *ApJ*, 671, 1388
 de Grijs M. H. K., Keel W. C., Miley G. K., Goudfrooij P., Lub J., 1992, *Astronomy and Astrophysics Supplement Series* (ISSN 0365-0138), 96, 389
 Dressler A., Gunn J. E., 1983, *ApJ*, 270, 7
 Dunlop J. S., McLure R. J., Kukulka M. J., Baum S. A., O’Dea C. P., Hughes D. H., 2003, *MNRAS*, 340, 1095
 Emonts B. H. C., Morganti R., Tadhunter C. N., Holt J., Oosterloo T. A., van der Hulst J. M., Wills K. A., 2006, *A&A*, 454, 125
 Ferrarese L., Ford H., 2005, *Space Science Reviews*, 116, 523
 Ferrarese L., Merritt D., 2000, *ApJL*, 539, L9
 Filippenko A. V., Ho L. C., 2003, *ApJ*, 588, L13
 Freedman Woods D., Geller M. J., Kurtz M. J., Westra E., Fabricant D. G., Dell’Antonio I., 2010, *arXiv*, arXiv:1002.0386
 Gadotti D. A., 2009, *MNRAS*, 393, 1531
 Gadotti D. A., Kauffmann G., 2009, *mnras*, p. 1121
 Gallazzi A., Charlot S., Brinchmann J., White S. D. M., 2006, *MNRAS*, 370, 1106
 Gallo E., Treu T., Jacob J., Woo J.-H., Marshall P. J., Antonucci R., 2008, *ApJ*, 680, 154
 Gebhardt K., Bender R., Bower G., et al., 2000, *ApJL*, 539, L13
 González Delgado R. M. G., Heckman T., Leitherer C., 2001, *ApJ*, 546, 845
 Goto T., 2006, *MNRAS*, 369, 1765
 Graham A. W., Li I. H., 2009, *ApJ*, 698, 812
 Haehnelt M. G., Natarajan P., Rees M. J., 1998, *MNRAS*, 300, 817
 Hao L., Strauss M. A., Fan X., et al., 2005, *AJ*, 129, 1795
 Häring N., Rix H.-W., 2004, *ApJ*, 604, L89
 Heckman T. M., Gonzalez-Delgado R., Leitherer C., Meurer G. R., Krolik J., Wilson A. S., Koratkar A., Kinney A., 1997, *ApJ*, 482, 114
 Heckman T. M., Kauffmann G., Brinchmann J., Charlot S., Tremonti C., White S. D. M., 2004, *ApJ*, 613, 109
 Heckman T. M., Ptak A., Hornschemeier A., Kauffmann G., 2005, *ApJ*, 634, 161
 Ho L. C., Filippenko A. V., Sargent W. L. W., 1997, *ApJ*, 487, 568
 Hopkins P. F., Hernquist L., 2009, eprint arXiv0910:4582
 Hopkins P. F., Hernquist L., Cox T. J., Matteo T. D., Robertson B., Springel V., 2006, *ApJS*, 163, 1
 Hu J., 2008, *MNRAS*, 386, 2242
 Johansson P. H., Naab T., Burkert A., 2009, *ApJ*, 690, 802
 Kauffmann G., Heckman T. M., 2009, *MNRAS*, 397, 135

- Kauffmann G., Heckman T. M., Tremonti C., et al., 2003, MNRAS, 346, 1055
- Kennicutt R. C., 1998, ARAA, 36, 189
- Kewley L. J., Dopita M. A., Sutherland R. S., Heisler C. A., Trevena J., 2001, ApJ, 556, 121
- Kewley L. J., Geller M. J., Barton E. J., 2006, AJ, 131, 2004
- Kewley L. J., Groves B., Kauffmann G., Heckman T., 2006, MNRAS, 372, 961
- Khalatyan A., Cattaneo A., Schramm M., Gottlöber S., Steinmetz M., Wisotzki L., 2008, MNRAS, 387, 13
- Marconi A., Hunt L. K., 2003, ApJ, 589, L21
- Matteo T. D., Springel V., Hernquist L., 2005, Nature, 433, 604
- Mulchaey J. S., Koratkar A., Ward M. J., Wilson A. S., Whittle M., Antonucci R. R. J., Kinney A. L., Hurt T., 1994, ApJ, 436, 586
- Norman C., Scoville N., 1988, ApJ, 332, 124
- Osterbrock D. E., 1989, Astrophysics of gaseous nebulae and active galactic nuclei
- Panther B., Jimenez R., Heavens A. F., Charlot S., 2008, MNRAS, 391, 1117
- Paumard T., Genzel R., Martins F., et al., 2006, ApJ, 643, 1011
- Poggianti B. M., Wu H., 2000, ApJ, 529, 157
- Rupke D. S. N., Kewley L. J., Barnes J. E., 2010, arXiv, arXiv:1001.1728
- Sanders D. B., Soifer B. T., Elias J. H., Madore B. F., Matthews K., Neugebauer G., Scoville N. Z., 1988, ApJ, 325, 74
- Schawinski K., Thomas D., Sarzi M., Maraston C., Kaviraj S., Joo S. J., Yi S. K., Silk J., 2007, MNRAS, 382, 1415
- Silk J., Rees M. J., 1998, A&A, 331, L1
- Strauss M. A. et al. (The SDSS Collaboration), 2002, AJ, 124, 1810
- Tadhunter C. N., Dickson R. C., Shaw M. A., 1996, MNRAS, 281, 591
- Tremaine S., Gebhardt K., Bender R., et al., 2002, ApJ, 574, 740
- Tremonti C. A., Heckman T. M., Kauffmann G., et al., 2004, ApJ, 613, 898
- Veilleux S., 2001, Starburst Galaxies: Near and Far, p. 88
- Wild V., Kauffmann G., Heckman T., Charlot S., Lemson G., Brinchmann J., Reichard T., Pasquali A., 2007, MNRAS, 381, 543
- Wild V., Walcher C. J., Johansson P. H., Tresse L., Charlot S., Pollo A., Fèvre O. L., de Ravel L., 2009, MNRAS, 395, 144
- York D. G., Adelman J., Anderson J., et al, 2000, AJ, 120, 1579
- Yu Q., Tremaine S., 2002, MNRAS, 335, 965
- Zakamska N. L., Strauss M. A., Krolik J. H., et al., 2003, AJ, 126, 2125

APPENDIX A: SDSS IMAGES OF STARBURSTS

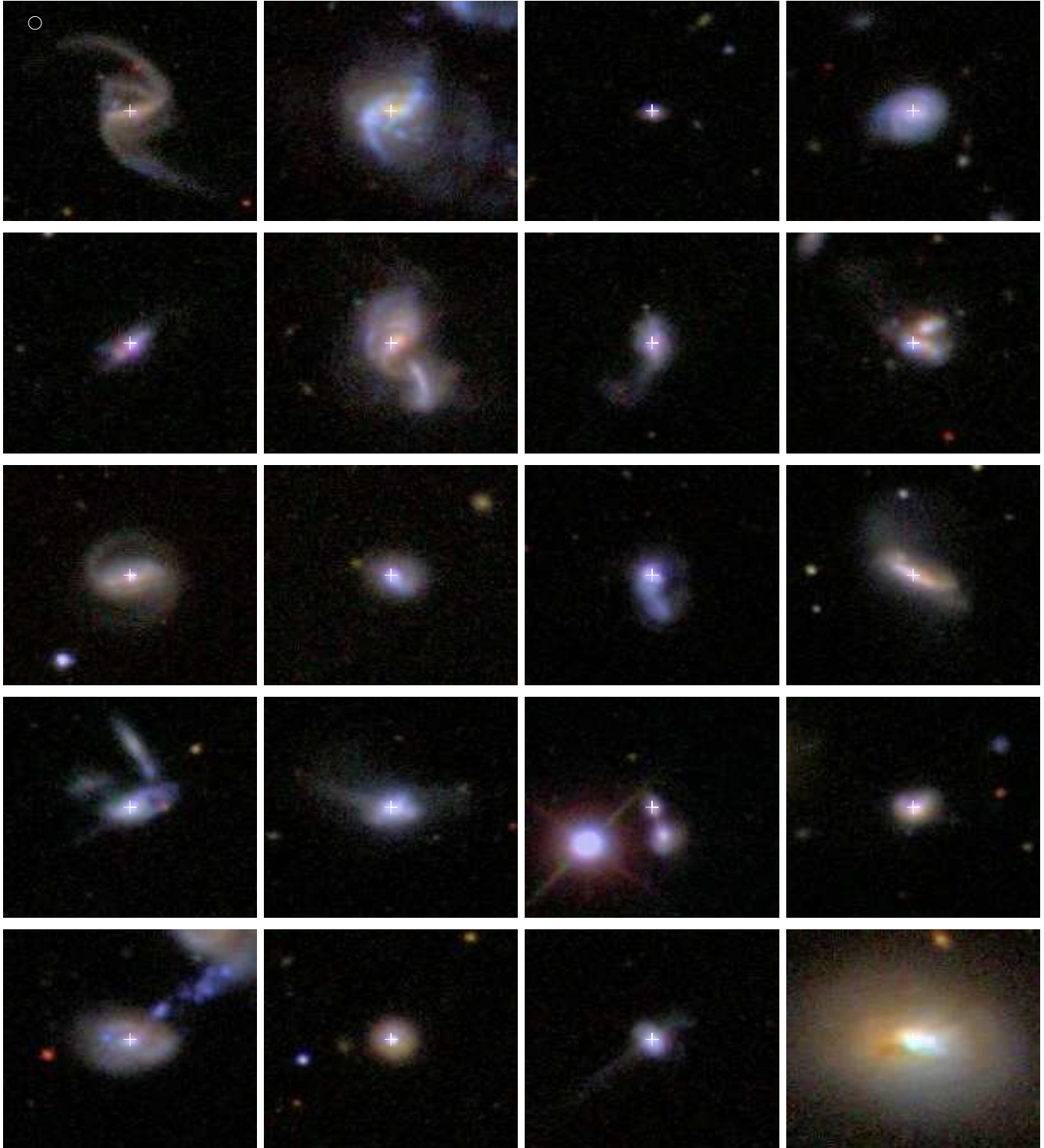


Figure A1. SDSS postage stamp images of the 20 youngest starbursts in our sample, each is $1'$ across. In the top left the white circle shows the size of the SDSS fibre through which the spectra are obtained. The white cross indicates the center of the image and approximate position of the fibre.

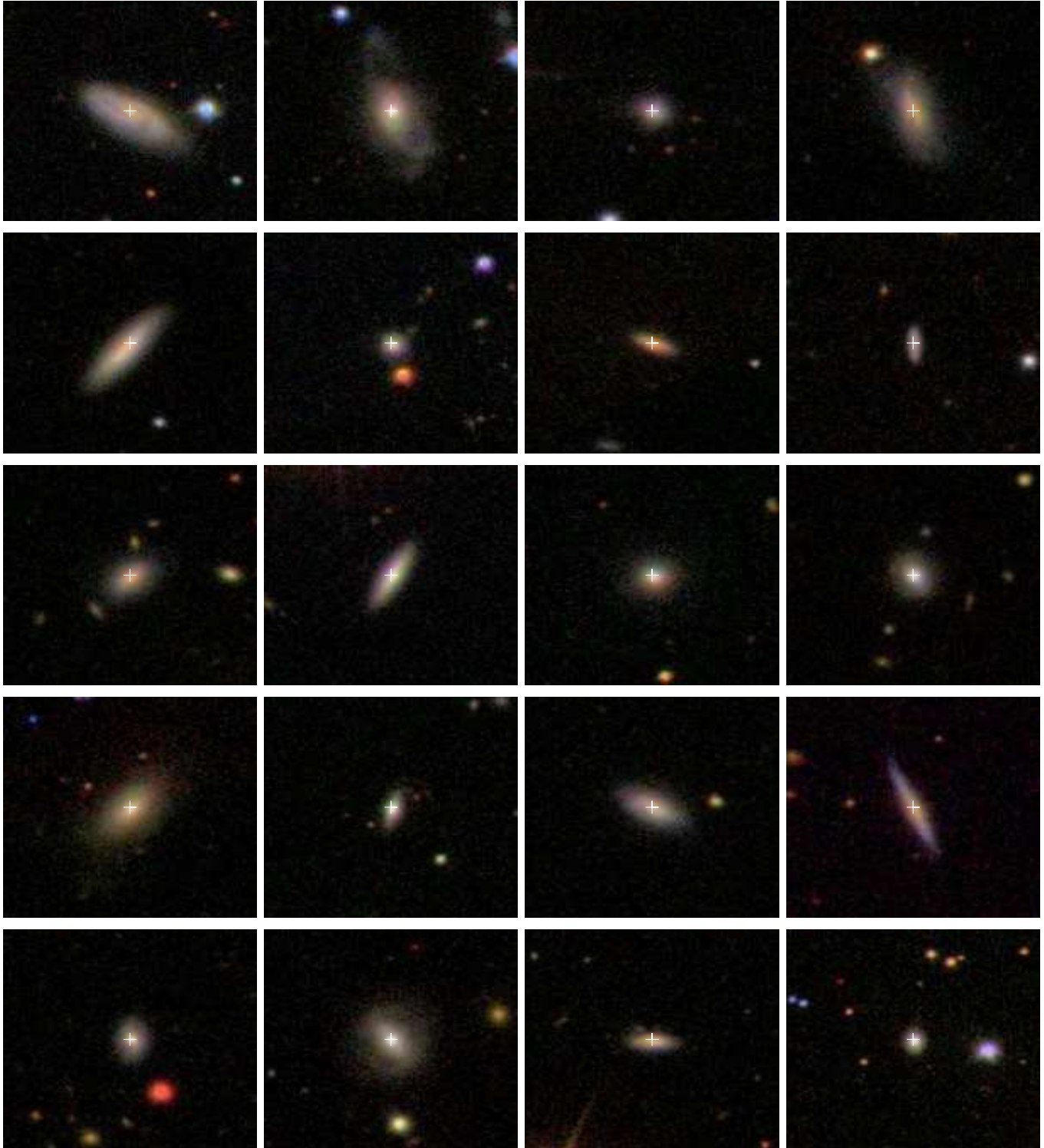


Figure A2. 1' SDSS postage stamp images of the 20 oldest starbursts in our sample.